Supporting Information

Crafting core-shell heterostructures of carbon nanotubes and N,O-coordinated cobalt sites-impregnated conjugated porous polymers for highly-efficient oxygen reduction

Rui Ma,‡[b] Zhengjiao Xie,‡[b] XiaoXue Xu,[a] Chenglong Tang,[b] Xueqin Liu,[a] Yunhai Zhu,[a] Xun Cui[a] and Yingkui Yang*[a,b]*

[a] State Key Laboratory of New Textile Materials and Advanced Processing Technologies, Wuhan Textile University, Wuhan 430200, China.

[b] School of Chemistry and Materials Science, South-Central Minzu University, Wuhan 430074, China.

‡ These two authors contributed equally to this work.

*Corresponding authors. E-mail: xcui@wtu.edu.cn; ykyang@wtu.edu.cn

The Supporting Information file includes:

1. Experimental Section

2. Figures

3. Tables

1. Experimental Section

1.1 Synthesis of Co-N,O-CPs

In a typical synthesis, 16 mg of 1,2-diaminobenzene (DB) and 21 mg of 1,3,5-triformylphloroglucinol (TP) with a molar ratio of 3:2 were mixed and stirred in 4 mL of DMF for 1h. Subsequently, the solution obtained by dissolving 40 mg of cobalt acetate tetrahydrate ($Co(CH_3COO)_2 \cdot 4(H_2O)$) in 1.5 mL of DMF was slowly added to the above solution under continuous stirring at room temperature. After stirring for 30 min, the above system was then transferred into a round-bottom flask and heated to 120 ℃ for 72 h under agitation and argon protection. Finally, the product (i.e., Co-N,O-CPs) was filtered, thoroughly washed with DMF, THF, deionized water and ethanol, and dried at 90 ℃ under vacuum overnight.

1.2 Synthesis of CNTs/N,O-CPs

In a typical synthesis, 16 mg of DB, 21 mg of TP, and 25 mg of CNTs (hydroxyl functionalized multi-walled carbon nanotubes, TNMPH1, TimesNano, 5-15 nm in outer diameter, 10-30 μm in length) were mixed and stirred in 5 mL of DMF to obtain a homogeneously dispersed solution. After stirring and sonication for 2 h, the above system was then transferred into a round-bottom flask and heated to 120 ℃ for 72 h under agitation and argon protection. Finally, the product (i.e., CNTs/N,O-CPs) was filtered, thoroughly washed with DMF, THF, deionized water and ethanol, and dried at 90 ℃ under vacuum overnight.

1.3 Synthesis of CNTs/Co-N,O-CPs

In a typical synthesis, 16 mg of DB, 21 mg of TP, and 25 mg of CNTs were mixed and stirred in 5 mL of DMF to obtain a homogeneously dispersed solution. After stirring and sonication for 2 h, the solution obtained by dissolving 40 mg of $Co(CH_3COO)_2 \cdot 4(H_2O)$ in 1.5 mL of DMF was slowly added to the above solution under continuous stirring at room temperature. After another stirring for 30 min, the above system was then transferred into a round-bottom flask and heated to 120 ℃ for 72 h under agitation and argon protection. Finally, the product (i.e., CNTs/Co-N,O-CPs) was filtered, thoroughly washed with DMF, THF, deionized water and ethanol, and dried at 90 ℃ under vacuum overnight.

1.4 Synthesis of CNTs/Co-N-CPs

In a typical synthesis, 33.8 mg of Tetraaminophenyl porphyrin (TAPP), 13.6 mg of Terephthalaldehyde (TPA) and 25 mg of CNTs were mixed and stirred in 5 mL of DMAC to obtain a homogeneously dispersed solution. After stirring and sonication for 2 h and addition of 250 uL of 6 M acetic acid solution, the above system was then transferred into a round-bottom flask and heated to 120 ℃ for 72 h under agitation and argon protection. The resulting CNTs/N-CPs was filtered, thoroughly washed with DMAC, THF and ethanol, and dried at 90 ℃ under vacuum overnight. After that, the CNTs/N-CPs and a certain amount of $Co(CH_3COO)_2 \cdot 4(H_2O)$ were mixed and stirred in 10 mL of ethanol and heated to 60℃ for 24 h. Finally, the product (i.e., CNTs/Co-N-CPs) was filtered, thoroughly washed with deionized water and ethanol, and dried at 90 ℃ under vacuum overnight.

1.5 Materials Characterizations

The morphology and structure of as-synthesized catalysts were investigated by scanning electron microscopy (SEM, Hitachi HT7700) and transmission electron microscopy (TEM, JEOL JEM-2100 F). The high-angle annular dark-field scanning transmission electron microscopy (HAADF-STEM) images were acquired by using a JEOL-2100F FETEM with electron acceleration energy of 250 kV. Fourier transfer infrared spectroscopy (FT-IR) spectra were obtained by a Thermo Nicolet NEXUS 470. The X-ray photoelectron spectroscopy (XPS) measurements were tested on a Thermo Scientific K-alpha photo-electron spectrometer (ESCALAB 250 Xi, Al Kα radiation). The binding energies (BE) were calibrated by setting the measured BE of C 1 s to 284.8 eV. The Brunauer-Emmett-Teller (BET) specific surface area and pore-size distribution were analyzed by nitrogen adsorption-desorption experiments at 77 K based on the instrument of ASAP 2020 PLUS HD88. X-ray diffraction (XRD) patterns were recorded on a Rigaku Miniflex 600 system (Cu Kα radiation, λ=1.5418 Å). XAFS spectra at the Co K-edge was collected at BL 14W1 station at Shanghai Synchrotron Radiation Facility (SSRF).

1.6 Electrochemical Measurements

The electrochemical measurements were conducted on the CHI 760E electrochemical workstation at room temperature. The glassy carbon rotating disk electrode (5.0 mm of diameter, 0.196 cm^2) coated with catalyst film was used as working electrode with Ag/AgCl (saturated KCl) and graphite rod as the reference and counter electrodes, respectively. All the potential was converted to the reversible hydrogen electrode (RHE) according to the Nernst equation ($E_{RHE} = E_{(Ag/AgCl)} + 0.0591 \times pH + 0.197$) in this work. The catalyst ink was prepared by mixing 5 mg of catalyst powder, 650 μL of deionized water, 300 μL of ethanol, and 50 μL of Nafion solution (5 wt%) and sonicating for 2 h. The cyclic voltammetry (CV) measurements were performed with a sweep rate of 20 mV s^{-1} in N_2- and O_2-saturated 0.1 M KOH solution. The linear sweep voltammetry (LSV) tests were recorded at a sweep rate of 10 mV s^{-1} with rotating speeds from 400 to 1600 rpm. The loading amounts of all catalysts including commercial Pt/C (20 wt%) were 0.20 mg cm^{-2}. Before testing, the electrolyte was saturated with N_2 or O_2 for at least 30 min. The long-term durability tests and methanol resistance were evaluated by chronoamperometry in O_2-saturated electrolyte with a rotation speed of 1600 rpm at the half-wave potential. The rotating ring disk electrode (RRDE) was used to assess the peroxide (H_2O_2) yield and electron transfer number (n) based on the below equations:

$$H_2O_2\% = 200 \frac{I_r/N}{I_d + I_r/N}$$

$$N = 4 \frac{I_d}{I_d + I_r/N}$$

Where I_r, I_d, and N are the ring current, disk current, and collection efficiency of Pt ring (N=0.37, provided by the manufacturer), respectively. The electron transfer number (n) was also calculated by using the following Koutecky-Levich (K-L) equation:

$$\frac{1}{J} = \frac{1}{J_L} + \frac{1}{J_K} = \frac{1}{B\omega^{0.5}} + \frac{1}{J_K}$$

$$B = 0.2nFC_0(D_0)^{2/3}\upsilon^{-1/6}$$

where J, J_L, and J_K are the measured current density, diffusion limited current density, and kinetic limited current density, respectively. ω is the rotating speed (rpm), n is the electron transfer number, F is the Faraday constant (96, 485 C mol^{-1}), C_0 is the bulk

concentration of O_2 (1.2×10^{-3} mol L^{-1}), D_0 is the diffusion coefficient of O_2 (1.9×10^{-5} cm^2 s^{-1}), and ν is the kinematic viscosity of the electrolyte (0.01 cm^2 s^{-1}).

1.7 Zinc-air battery measurements

The zinc-air battery measurements were conducted on a home-made electrochemical liquid battery. The carbon paper coated with CNTs/Co-N,O-CPs or Pt/C (20 wt%) and polished zinc plate (purity > 99.9%, thickness: 0.5 mm) were used as the air cathode and anode, respectively. The loading amount of CNTs/Co-N,O-CPs and Pt/C on carbon paper is 1.0 mg cm^{-2}. A mixed solution of 6.0 M KOH and 0.2 M $Zn(CH_3COO)_2$ solution was used as the electrolyte. All the measurements were carried out on the home-made battery at the room temperature with an electrochemical workstation (CHI 760E).

1.8 DFT calculations

The first principle Density functional theory (DFT) calculations are performed by Vienna Ab initio Simulation Package (VASP)[1, 2] with the projector augmented wave (PAW)[3] method. The exchange-functional is treated using the generalized gradient approximation (GGA) of Perdew-Burke-Ernzerhof (PBE) functional.[4] The energy cutoff for the plane wave basis expansion was set to 400 eV and the force on each atom less than 0.02 eV/Å was set for convergence criterion of geometry relaxation. To simulate the metal-nitrogen-doped carbon materials, a 6 × 6 graphene supercell was employed with ~15 Å vacuum space added in z-direction to avoid the periodical interactions. The Brillouin zone integration is performed using 3 × 3 × 1 gamma-centered k-point sampling through all the computational process. The self-consistent calculations apply a convergence energy threshold of 10^{-5} eV. The free energy diagrams for ORR were calculated with reference to the computational hydrogen electrode (CHE).[5] The CHE model uses one half of the chemical potential of gaseous hydrogen ($\mu(H_2)$) as the chemical potential of the proton-electron pair ($\mu(H^+/e^-)$). The free energy of each species can be obtained from the equation:

$$\Delta G = \Delta E_{DFT} + \Delta E_{ZPE} - T\Delta S$$

Where the ΔE_{DFT} is the reaction energy from DFT calculations, and the ΔE_{ZPE} and $T\Delta S$ are the change in the zero-point energy and entropy at room temperature (T=298.15 K), which are obtained after frequency calculations.

The ORR reaction proceeds with a $4e^-$ pathway are shown as follows:

$$O_2\,(g) + * + e^- + H_2O\,(l) \rightarrow *OOH + OH^- \quad (1)$$

$$*OOH + e^- \rightarrow *O + OH^- \quad (2)$$

$$*O + H_2O\,(l) + e^- \rightarrow *OH + OH^- \quad (3)$$

$$*OH + e^- \rightarrow OH^- + * \quad (4)$$

Where * refers to an active site on the catalysts surface.

References

[1] G. Kresse and J. Furthmüller, *Phys. Rev. B*, 1996, **54**, 11169-11186.
[2] G. Kresse and J. Furthmüller, *Comput. Mater. Sci.*, 1996, **6**, 15-50.
[3] G. Kresse and D. Joubert, *Phys. Rev. B*, 1999, **59**, 1758-1775.
[4] J. P. Perdew, K. Burke and M. Ernzerhof, *Phys. Rev. Lett.*, 1996, **77**, 3865-3868.
[5] J. K. Nørskov, J. Rossmeisl, A. Logadottir, L. Lindqvist, J. R. Kitchin, T. Bligaard and H. Jonsson, *J. Phys. Chem. B*, 2004, **108**, 17886-17892.

2. Figures

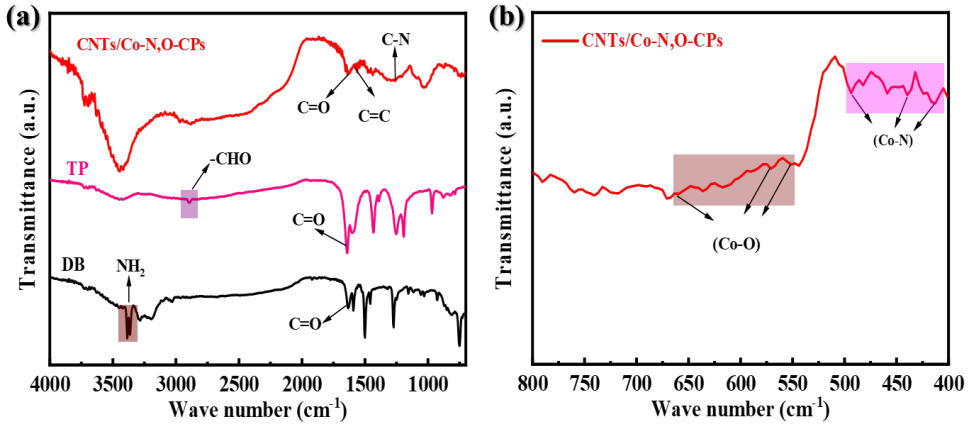

Figure S1. (a) FTIR spectra of TP, DB, and CNTs/Co-N,O-CPs in the wave number range of 700 to 4000 cm^{-1}, (b) FTIR spectrum of CNTs/Co-N,O-CPs in the wave number range of 400 to 800 cm^{-1}.

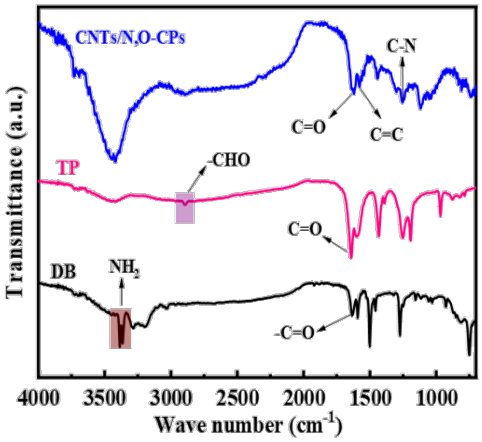

Figure S2. FTIR spectra of TP, DB, and CNTs/N,O-CPs.

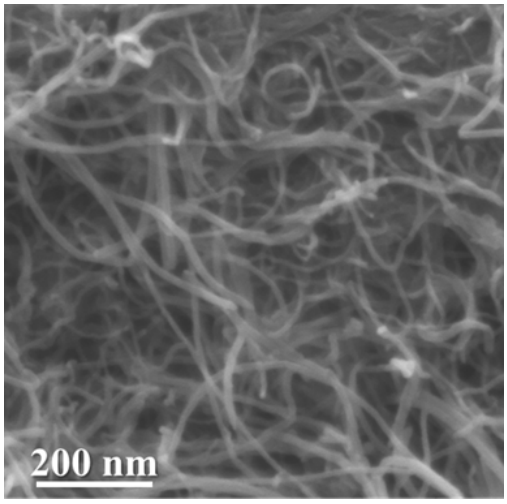

Figure S3. SEM image of the pristine CNTs.

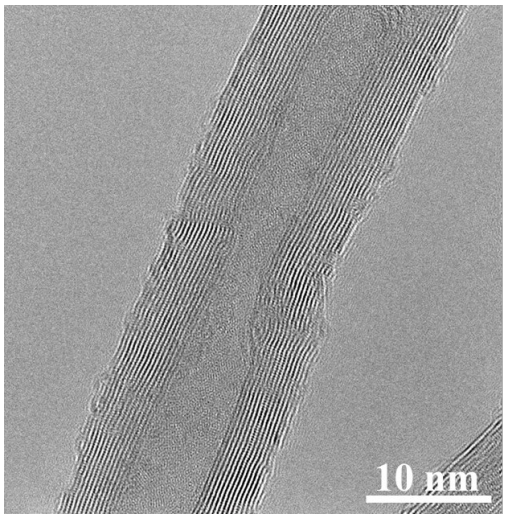

Figure S4. TEM image of pristine CNTs.

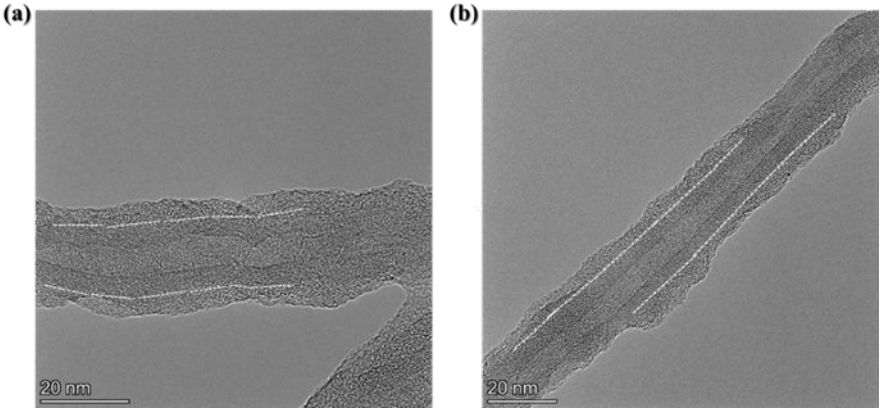

Figure S5. TEM images of CNTs/Co-N,O-CPs.

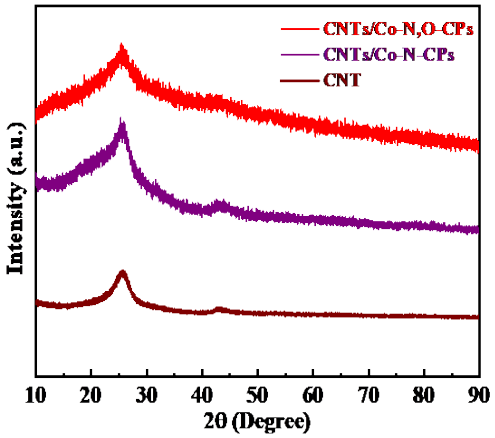

Figure S6. XRD patterns of CNTs/Co-N,O-CPs, CNTs/Co-N-CPs, and pristine CNTs.

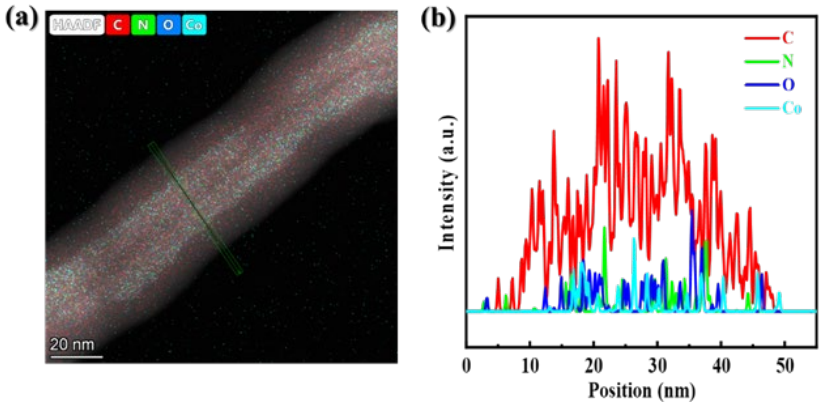

Figure S7. (a) HAADF-STEM image and EDX area-scan profile, (b) EDX line-scan profile of CNTs/Co-N,O-CPs.

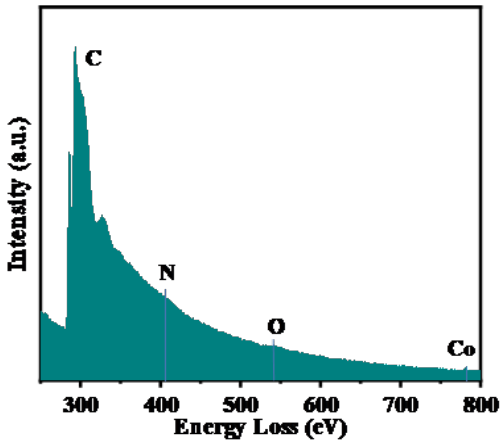

Figure S8. EELS spectrum of CNTs/Co-N,O-CPs.

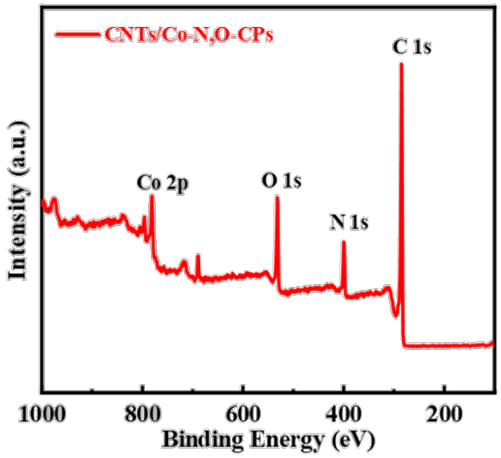

Figure S9. XPS survey spectrum of CNTs/Co-N,O-CPs.

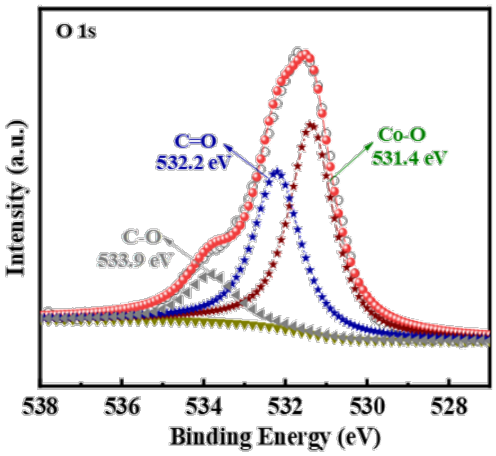

Figure S10. High-resolution XPS spectrum of O 1s of CNTs/Co-N,O-CPs.

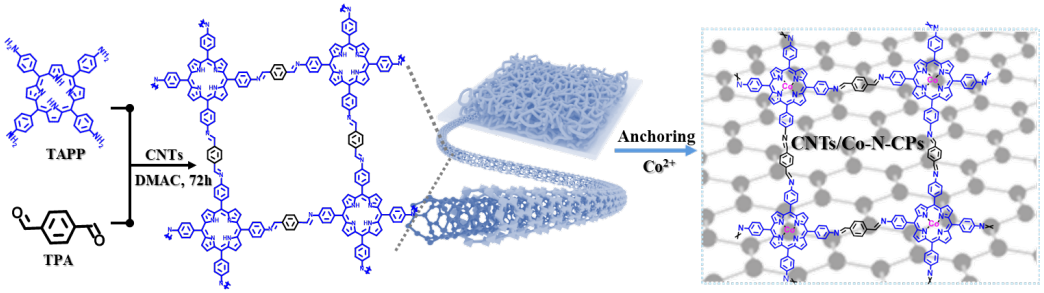

Figure S11. Schematic illustration for the synthesis of CNTs/Co-N-CPs.

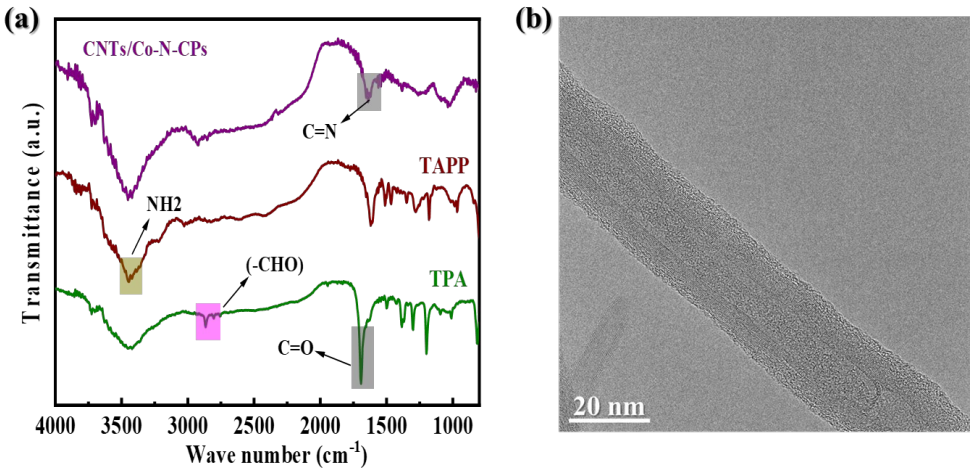

Figure S12. (a) FTIR spectra of TAPP, TPA and CNTs/Co-N-CPs, (b) TEM image of CNTs/Co-N-CPs.

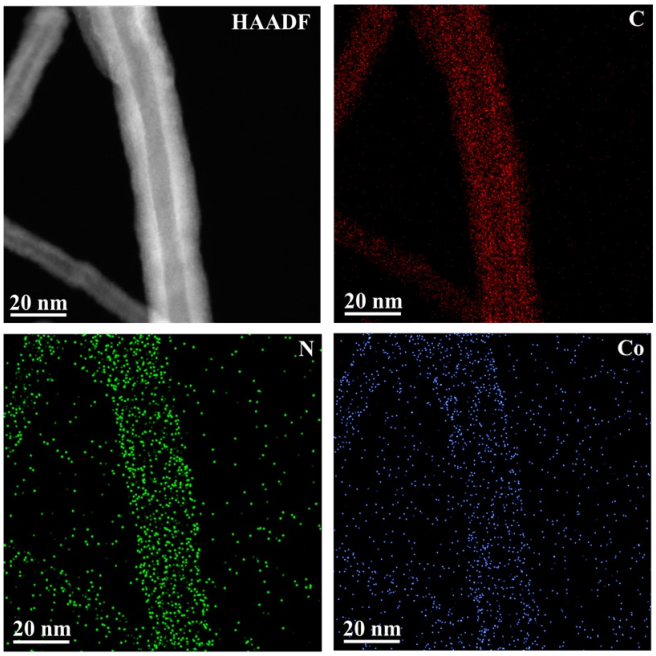

Figure S13. HAADF-STEM and EDX elemental mapping images of CNTs/Co-N-CPs.

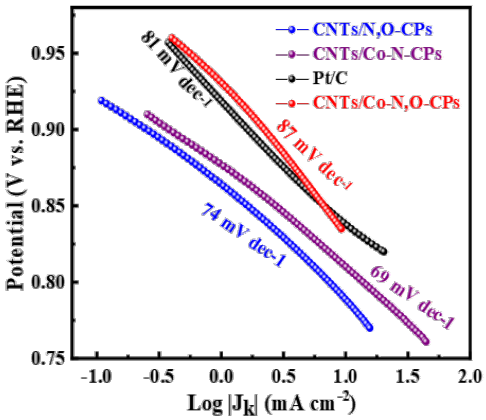

Figure S14. Tafel plots of CNTs/Co-N,O-CPs, CNTs/Co-N-CPs, CNTs/N,O-CPs, and Pt/C.

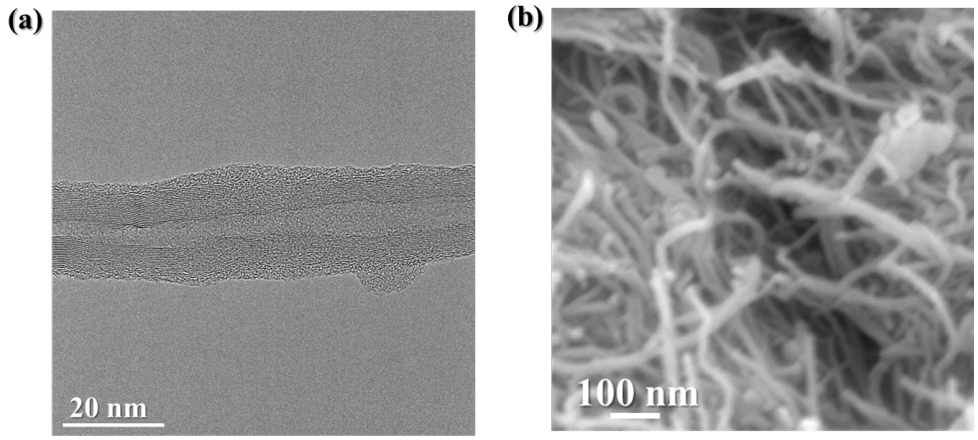

Figure S15. (a) TEM and (b) SEM images of CNTs/N,O-CPs.

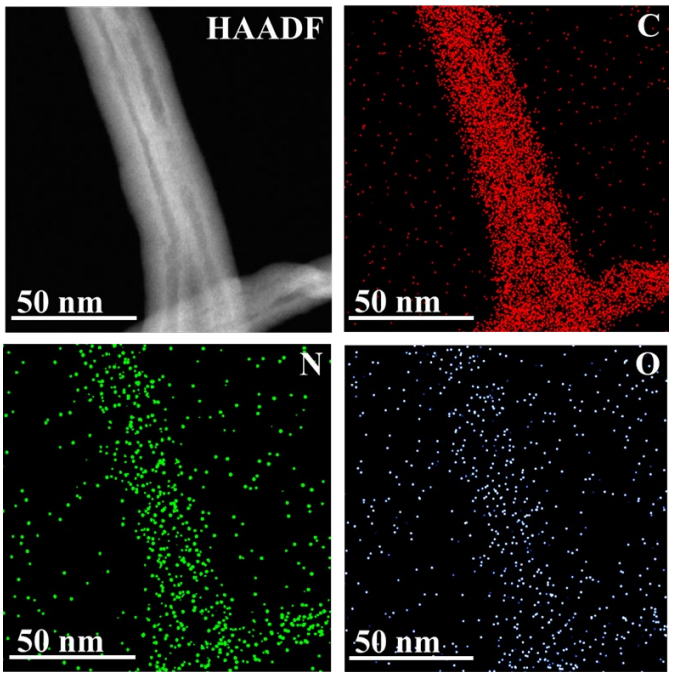

Figure S16. HAADF-STEM and EDX elemental mapping images of CNTs/N,O-CPs.

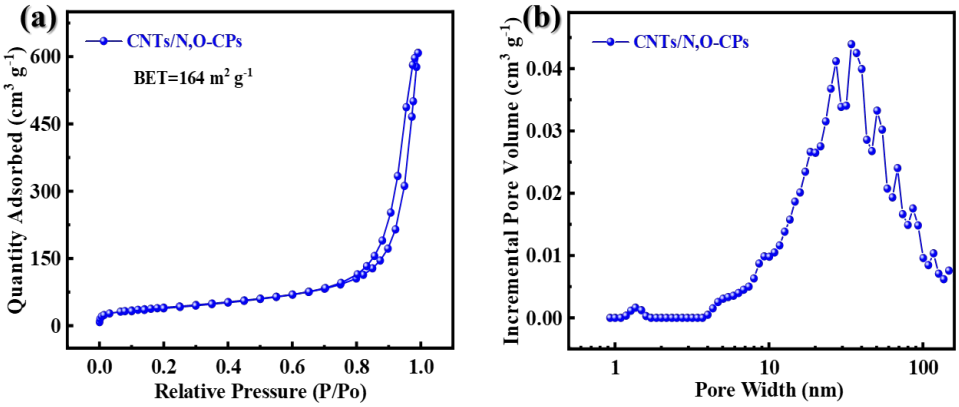

Figure S17. (a) Nitrogen adsorption-desorption isotherms and (b) pore-size distribution of CNTs/N,O-CPs.

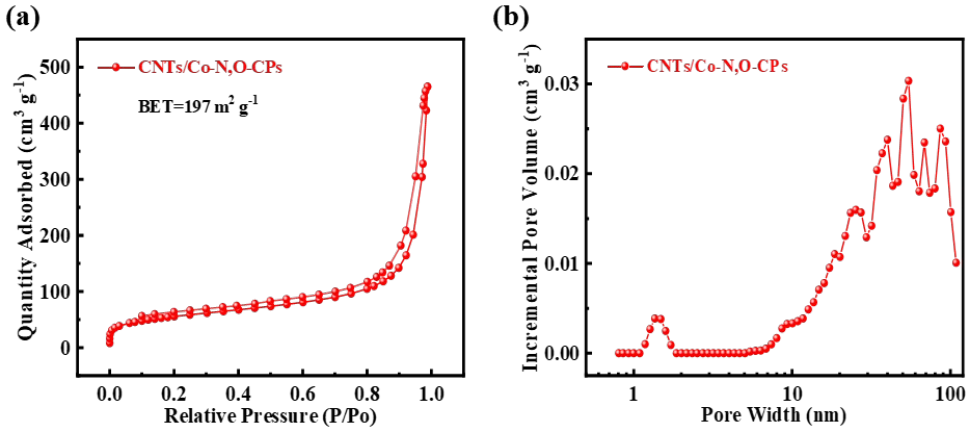

Figure S18. (a) Nitrogen adsorption-desorption isotherms and (b) pore-size distribution of CNTs/Co-N,O-CPs.

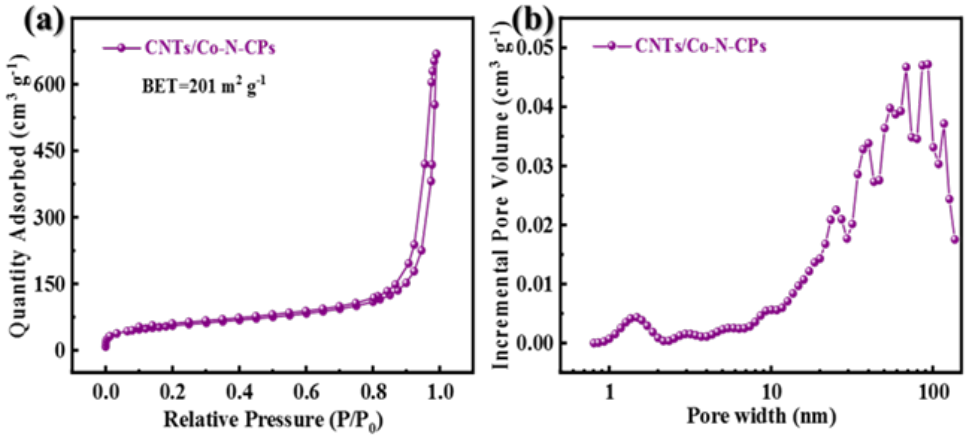

Figure S19. (a) Nitrogen adsorption-desorption isotherms and (b) pore-size distribution of CNTs/Co-N-CPs.

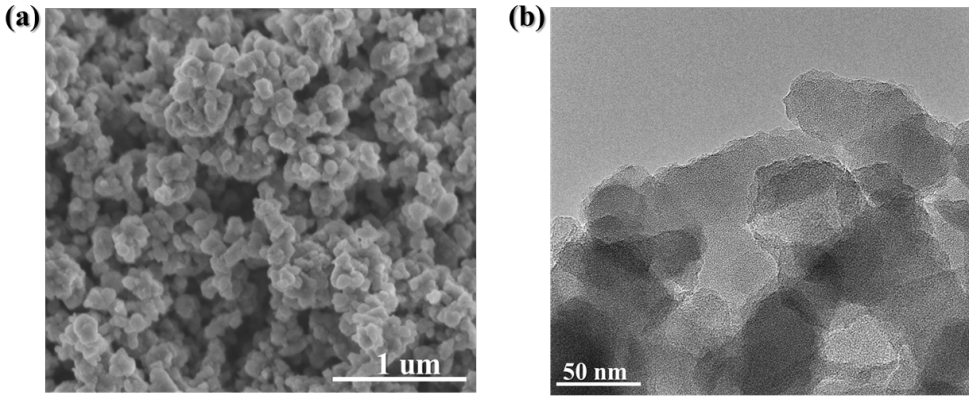

Figure S20. (a) SEM and (b) TEM images of Co-N,O-CPs.

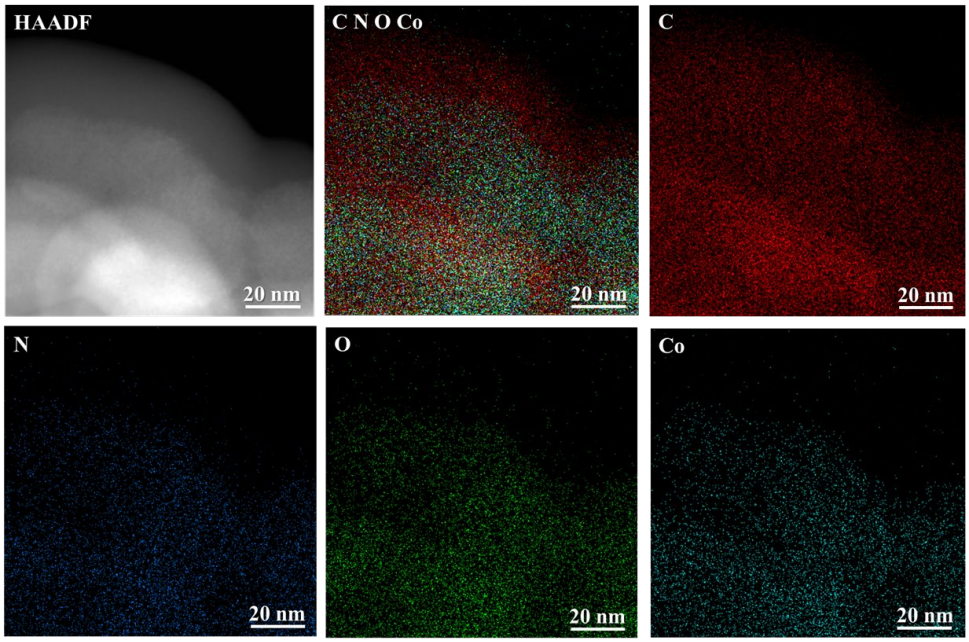

Figure S21. HAADF-STEM and EDX element mapping images of Co-N,O-CPs.

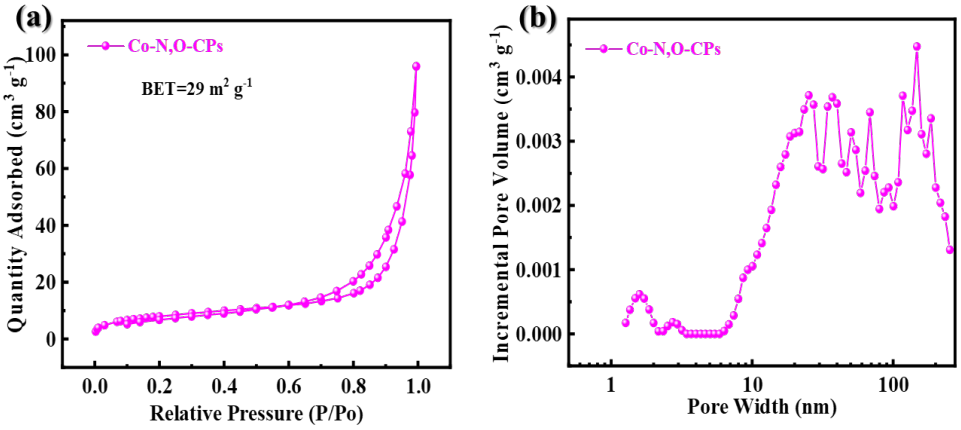

Figure S22. (a) Nitrogen adsorption-desorption isotherms and (b) pore-size distribution of Co-N,O-CPs.

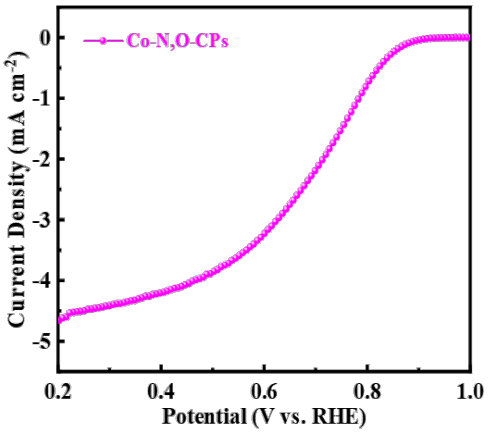

Figure S23. LSV curve of Co-N,O-CPs at a rotation speed of 1600 rpm.

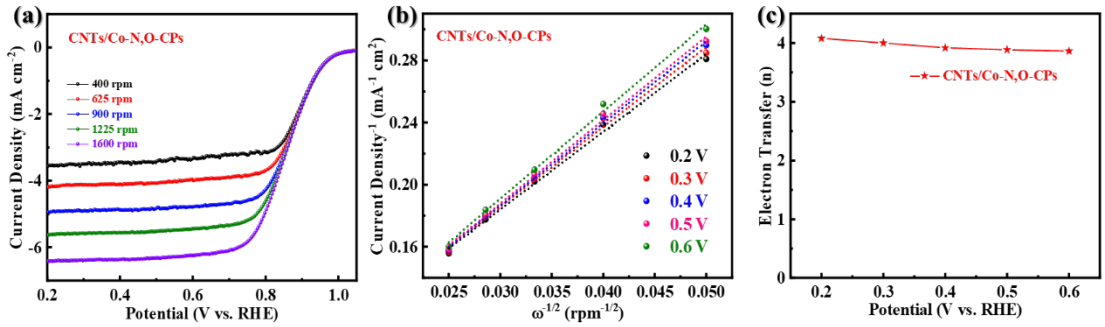

Figure S24. (a) LSV curves, (b) K-L plots, and (c) electron transfer numbers of CNTs/Co-N,O-CPs.

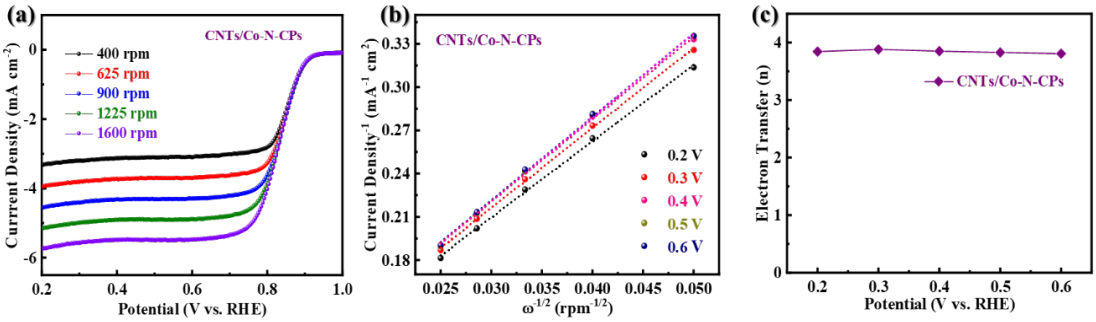

Figure S25. (a) LSV curves, (b) K-L plots, and (c) electron transfer numbers of CNTs/Co-N-CPs.

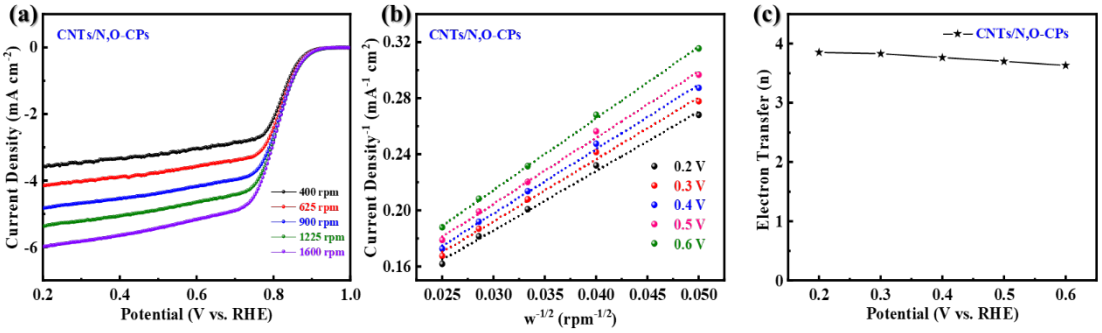

Figure S26. (a) LSV curves, (b) K-L plots, and (c) electron transfer numbers of CNTs/N,O-CPs.

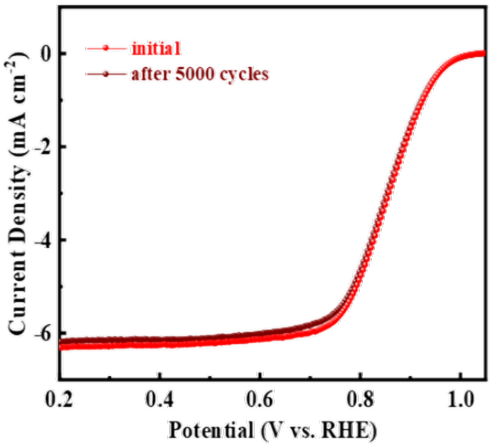

Figure S27. LSV curves of CNTs/Co-N,O-CPs before and after 5000 CV cycles.

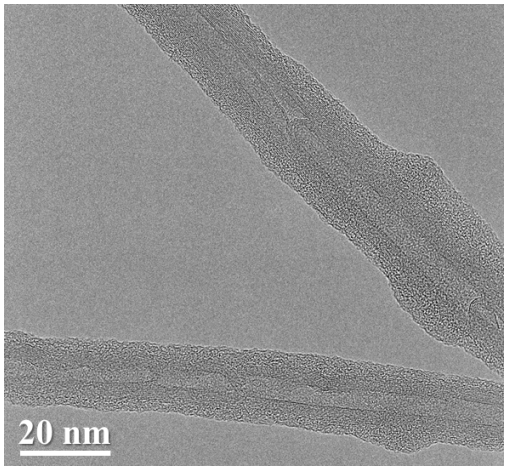

Figure S28. TEM image of CNTs/Co-N,O-CPs after durability test.

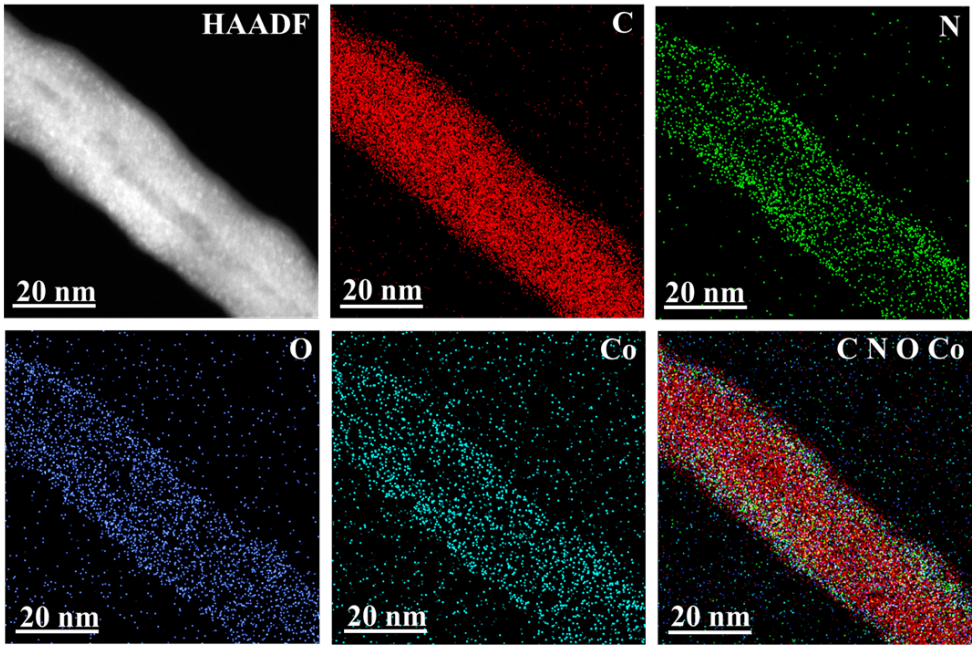

Figure S29. HAADF-STEM and EDX elemental mapping images of CNTs/Co-N,O-CPs after durability test.

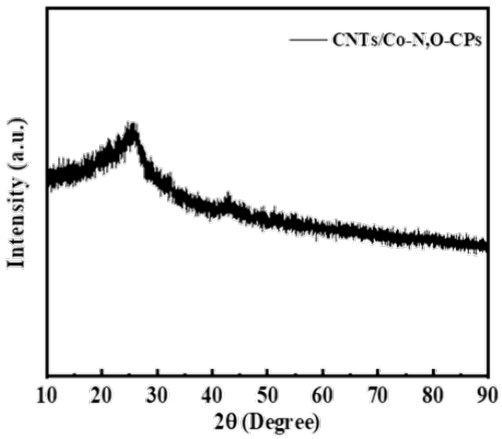

Figure S30. XRD pattern of CNTs/Co-N,O-CPs of after durability test.

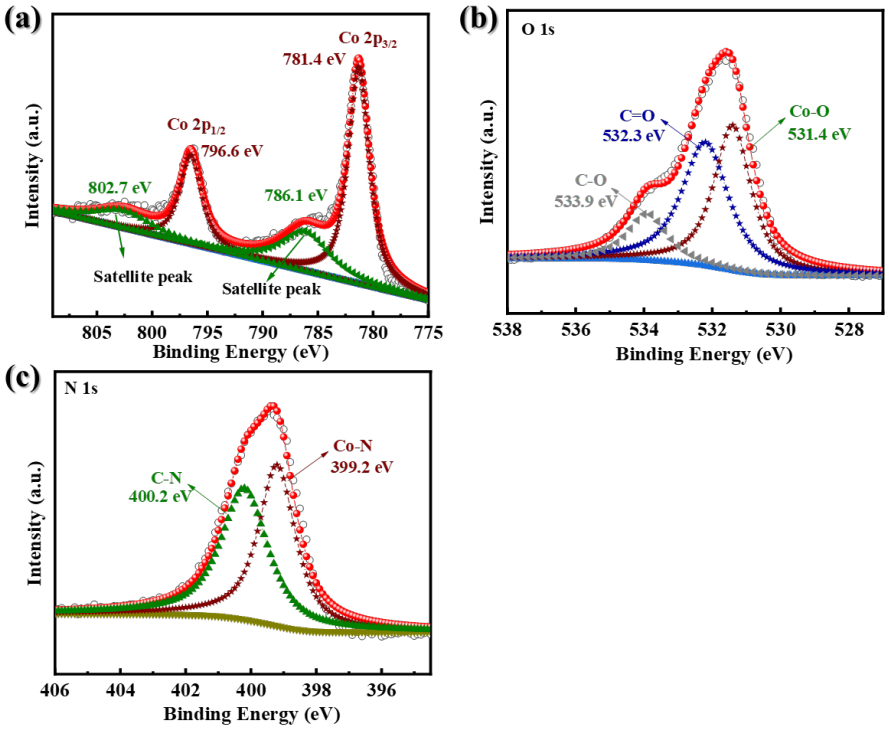

Figure S31. High-resolution XPS spectra of (a) Co 2p, (b) O 1s and (c) N 1s of CNTs/Co-N,O-CPs after durability test.

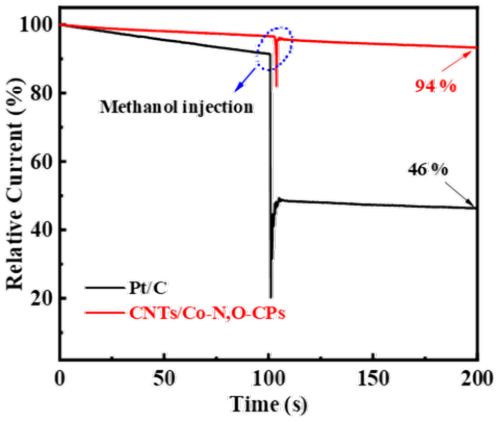

Figure S32. Chronoamperometric responses of CNTs/Co-N,O-CPs and Pt/C with the addition of methanol at approximately 100 s.

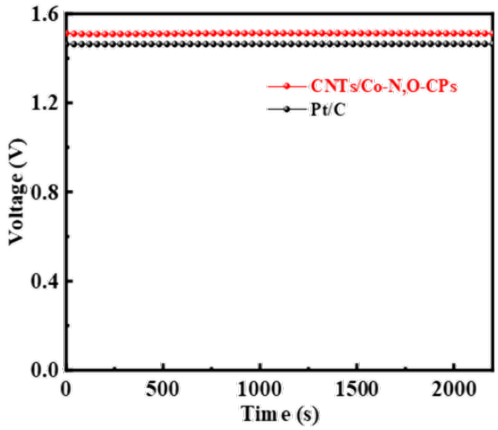

Figure S33. Open circuit potentials of CNTs/Co-N,O-CPs- and Pt/C-based Zn-air batteries.

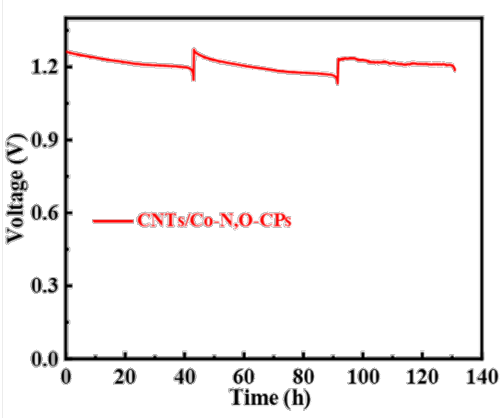

Figure S34. Long-term durability test of CNTs/Co-N,O-CPs-based zinc-air battery recharged by replacing the zinc anode and electrolyte.

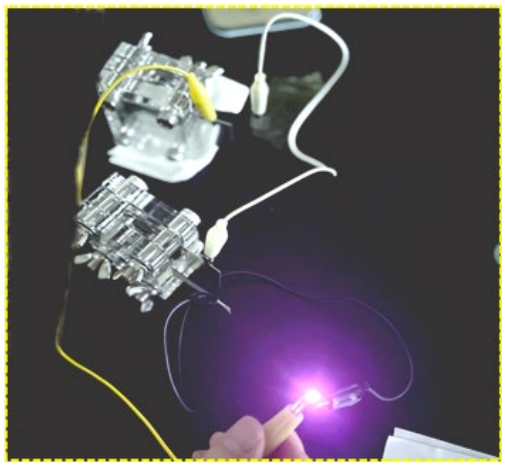

Figure S35. Photograph of a LED powered by two home-made zinc-air batteries with CNTs/Co-N,O-CPs as the air cathode.

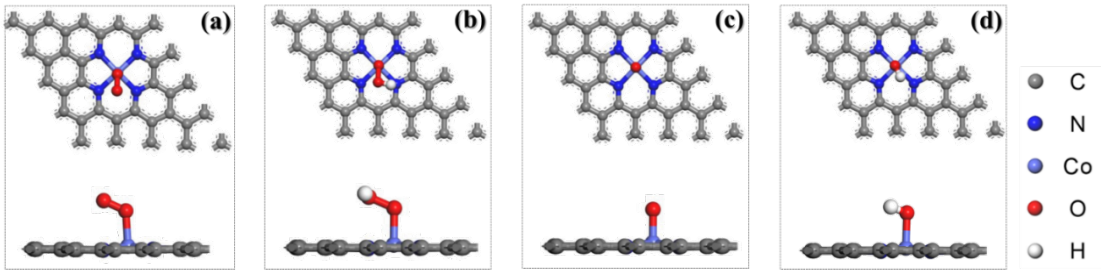

Figure S36. Optimized geometrical structures (top and side views) of (a) *OO, (b) *OOH, (c) *O, and (d) *OH adsorbed on Co-N_4.

3. Tables

Table S1. Structural parameters extracted from EXAFS fitting of CNTs/Co-N,O-CPs.

Sample	Edge	Path	CN	R(Å)	$\sigma^2(10^{-3}$ Å)	ΔE_0(eV)	R-factor
CNTs/Co-N,O-CPs	Co-K	Co-N	2.36	1.94	1.12	-5.90	0.015
		Co-O	2.26	2.09	1.08	2.68	

CN: coordination number; R: interatomic distance; σ^2: Debye-Waller factor; ΔE_0: inner potential correction; R-factor: goodness of the fitting.

Table S2. Comparison of various state-of-the-art electrocatalysts towards ORR and zinc-air batteries.

Catalyst	Spcific capacity (mAh g^{-1})	Power density (mW cm^{-2})	Half-wave potential ($E_{1/2}$ V vs. RHE)	Diffusion-limited current density (mA cm^{-2})	Electron transfer number (n)	Reference
CNTs/Co-N,O-CPs	814	181	0.868	6.30	≈4	This Work
Co-NCS-2	805	292	0.90	5.0	4	Nano Energy, 2021, **87**, 106153
Co-NCS-0	-	-	0.81	5.4	—	
Co SAs@PNCN	-	220	0.851	≈5.9	3.98	Small, 2022, **18**, 2202476
Co@NCNRs	-	76.76	0.835	5.697	4	Energy Environ. Mater., 2022, **0**, 1–7
Co- CoN_4@NCNs	776.7	118.8	0.83	6.0	3.8	Adv. Funct. Mater., 2022, **32**, 2207331
CoNi-CoN_4-HPC-900	-	116	0.78	6.85	4	Nano Energy, 2022, **99**, 107325
FePc&rGO	739.7	103	0.89	5.4	3.97	Energy Storage Mater., 2022, **50**, 12-20
Fe-N-C	775.7	175	0.895	5.8	≈4	Appl. Catal. B: Environ., 2022, **313**, 121454
Co-CMS	733.94	219	0.83	-	4	Adv. Energy Mater., 2022, **12**, 2103097
Mn-RuO_2	812	181	0.86	6.0	-	J. Am. Chem. Soc., 2022, **144**, 2694−2704
Ce-Co_3O_4	876.3	-	0.71	4.83	3.6	Adv. Funct. Mater., 2023, **33**, 2212021
Mo/C	771	197	0.810	5.24	4.0	J. Am. Chem. Soc., 2022, **144**, 20571−20581
Ni-B/N-C	700	175	0.87	6.1	3.94	Adv. Funct. Mater., 2023, 2213863
CNT@SAC-Co/NCP	864.8	172	0.870	5.4	3.91	Adv. Funct. Mater., 2021, **31**, 2103360
FeCo-NSC	782.1	152.8	0.86	5.26	3.98	Energy Storage Mater., 2022, **45**, 805–813
OLC/Co-N-C	790	238	0.855	5.5	3.8	Angew. Chem. Int. Ed., 2021, **60**, 12759 –12764

Table S3. BET specific surface area and pore volume of CNTs/Co-N,O-CPs and CNTs/N,O-CPs.

Sample	BET specific surface area ($m^2 g^{-1}$)	Pore volume ($cm^3 g^{-1}$)
CNTs/Co-N,O-CPs	197	0.94
CNTs/N,O-CPs	164	0.72
CNTs/Co-N-CPs	201	1.03
Co-N,O-CPs.	29	0.15